An Efficient Iterative Least Square Method for Indoor Visible Light Positioning Under Shot Noise

Xiaona Liu, Difan Zou, Nuo Huang, and Yang Wang

***Abstract*—In this paper, we develop a set of effective algorithms for performing efficient and accurate visible light positioning (VLP) in the presence of shot noise, which is an important component in the received optical signal yet has been largely neglected in prior works. In particular, we formulate the positioning problem as a maximum log-likelihood optimization problem, which is nonconvex so that the standard numerical algorithm such as gradient descent (GD) and stochastic gradient descent (SGD) may not be able to find the global solution. To address this, we propose a novel least-square (LS) solver that can find a sub-optimal solution to the aforementioned non-convex optimization problem. Based on the LS solver, a set of more effective algorithms can be developed to further enhance the optimality of the solution. Specifically, we consider (1) combining the LS solver with GD, giving rise to the GD-LS algorithm; and (2) applying the LS solver in an iterative manner, giving rise to the iterative LS algorithm, which is a novel and efficient positioning algorithm. Moreover, we also provide a closed-form lower bound on the positioning error based on the Cramér-Rao lower bounds (CRLB). Numerical simulation shows that the proposed GD-LS and iterative LS algorithms cannot only achieve high positioning accuracy, but also enjoy low computation complexity: the average positioning accuracy of LS-GD is 0.009 m using computation time 0.046 s, and the iterative LS algorithm can achieve average positioning accuracy 0.023 m with 1.94×10^{-4}s computation time, which outperform GD and SGD method.**

***Index Terms*—Visible light positioning, gradient descent, least square, CRLB.**

I. Introduction

NOWADAYS, indoor positioning system (IPS) is becoming increasingly critical in daily life. In shopping malls, hospitals, airports, parking lots, and other indoor venues, navigation and other location-based services (LBS) are indispensable in many aspects of daily life, businesses, and industry. As the present mainstream in positioning systems, Global Positioning System (GPS) has been widely adopted in aircraft, vehicles, and portable devices in order to provide real-time positioning and navigation [1]. Each GPS receiver knows the position of each satellite when the signal was transmitted. Meanwhile, it also measures the time differences of arrival (TDOA) of signals from each transmitter. Accordingly, the distance between the receiver to each transmitter can be estimated and the user's current position can be further obtained by using trilateration [2]. However, due to blockage and discontinuous signals, GPS is inaccurate in indoor scenarios. In particular, indoor positioning system (IPS) can be built using indoor wireless signals (e.g., WiFi [3], [4], Bluetooth [5], [6], radio frequency identification (RFID) [7], [8], and ZigBee [9]. Apart from the aforementioned indoor positioning techniques, visible light positioning (VLP) has attracted extensive attention from researchers due to its superior practical performance in recent years. VLP stems from visible light communication (VLC), where LEDs in the ceiling can both illuminate and transmit signals. Besides, VLC is able to adopt cost-effective, license-free, and electromagnetic interference-free optical spectrum, which can potentially offer significantly larger transmission rates compared with the RF spectrum. The commonly used transmission source of VLC is the ubiquitous light-emitting diode (LED), which is gaining popularity due to its low cost, low power consumption, wide modulation bandwidth, and long lifetime. LEDs efficiently serve the dual purposes of lighting and communication. In this context, wireless networking using VLC, which is referred to as Light Fidelity (LiFi), was introduced in 2011 [10] and has further been included in the IEEE standards [11]. In the VLP system, each LED has its unique ID and transmits distinct signals to the receiver. It has been observed in many works that VLP can provide accurate positioning services with $0.1 - 0.35$ m positioning error compared with WiFi ($1 - 7$ m), Bluetooth ($2 - 5$ m), and other technologies [12], [13], [14].

At the receiver side, the PD-based VLP system and camera-based system are the two most popular choices and have been widely studied and applied in practice. Most camera-based systems estimate the position using properties of the rolling shutters, which are found in the cameras of typical mobile phones. Some camera-based systems can achieve positioning accuracy by 3.2 cm [15]. Compared with camera-based systems, PDs have been shown to perform better in terms of stability, precision, and response time. A variety of systems are based on received signal strength (RSS), which are performed under the assumption that the receiver knows the transmitted power and radiation pattern of the luminaire. In [16], [17], the 3-D indoor VLP systems techniques using RSS are proposed and experimentally demonstrated based on the deep learning methods. Besides, A

Manuscript received 6 December 2022; accepted 10 December 2022. Date of publication 14 December 2022; date of current version 10 February 2023. This work was supported in part by Shenzhen Polytechnic under Grant 6021310025 K and in part by the Project of Science and Technology of Shenzhen under Grant GJHZ20200731095412038. *(Corresponding author: Yang Wang.)*

Xiaona Liu and Yang Wang are with the Institute of IoT, Shenzhen Polytechnic, Shenzhen 518055, China (e-mail: scarlett@mail.ustc.edu.cn; wyang@szpt.edu.cn).

Difan Zou is with the Department of Computer Science, the University of Hong Kong, Pokfulam 999077, Hong Kong (e-mail: dzou@hku.hk).

Nuo Huang is with the Optical Wireless Communication and Network Center, University of Science and Technology of China, Hefei 230026, China (e-mail: huangnuo@ustc.edu.cn).

Digital Object Identifier 10.1109/JPHOT.2022.3229052

passive indoor VLP system using deep learning is applied to the Internet of Things (IoT) scenario [18]. For more complex and non-Lambertian sources that traditional geometrical models are unsuited to determine the positions, the Gaussian Processes (GPs) are introduced in the context of RSS-based VLP [19], which are shown to work well when using small, noisy datasets for different applications.

Aside from the practical deployment of PD-based VLP system, a bunch of studies have theoretically characterized the accuracy limit based on Cramér-Rao lower bound (CRLB) [20], [21], [22], [23], [24], [25]. However, most of them concern the setting with only thermal noise, while ignoring the fact that in a real VLP system, there are multiple types of noises having non-negligible effects to the positioning accuracy. The most important one among them is the signal-dependent shot noise, which is shown to have a significant effect to the visible light communication system [26], especially in a "light-off" condition. In our previous work [27], we showed that the shot noise will drastically worsen the positioning accuracy of the VLP system, especially in the low signal-noise-ratio (SNR) regime. In our system.

In a variety of indoor positioning works, the GD algorithm has been utilized to solve for the optimal position based on the classical received signal strength (RSS) based trilateration [28]. However, when taking the shot noise into consideration, the training objective function (e.g., log-likelihood function) will become non-convex, preventing GD from finding the globally optimal solution. Motivated by this challenge, we first propose a novel least-square (LS) solver to obtain a sub-optimal solution, which will be further combined with GD or performed in an iterative manner to improve the optimality of the solution. To the best of our knowledge, this paper is the first attempt to discuss VLP under signal-dependent shot noise. We highlight the major contributions of this paper as follows:

- Most work neglect shot noise in VLP system, which may be the dominant opponent in optical communication systems. In our paper, the shot noise is considered in VLP system for a more practical and general case. Under this premise, we formulate the log-likelihood maximization problem for VLP and point out the drawbacks of the standard gradient descent algorithm.
- Based on the developed log-likelihood maximization problem, we develop a set of efficient and effective algorithms for finding the optimal positions. In particular, we propose a novel least-square (LS) solver that gives a sub-optimal solution. Accordingly, we further propose two algorithms: LS-GD, and iterative LS to further improve the positioning accuracy. Simulation results demonstrate the superior performance of the proposed algorithms: the LS-GD and iterative LS can not only achieve small positioning errors but also save the positioning running time costs.
- In addition to developing the positioning algorithms, we also derive a close-form lower bound on the positioning accuracy based on the Cramér-Rao lower bound, which provides a limit of the accuracy that can be achieved by any algorithm. Our simulation shows that the accuracy achieved by the proposed LS-GD algorithm has been quite close to the lower bound, which again verifies the effectiveness of the proposed positioning algorithms.

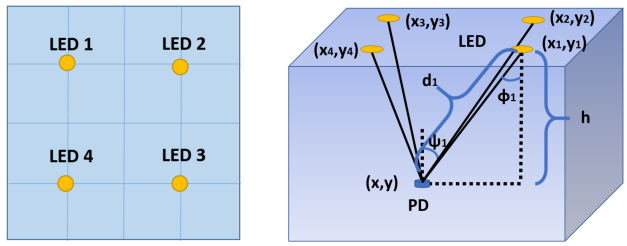

(a) Layout of LEDs (b) Diagram of the system

Fig. 1. The layout and diagram of the VLP system, where we display the case $M = 4$.

The remainder of this paper is organized as follows. We analyze the VLP system under thermal and shot noise in Section II. In Section III, we formulate the positioning task as a log-likelihood maximization problem and point out the drawbacks of the standard GD algorithm. In Section IV, we propose the LS solver for the log-likelihood maximization problem and develop the LS-GD and iterative LS algorithms accordingly. Meanwhile, we derive a closed-form lower bound of the positioning accuracy of the VLP system in Section V. Numerical simulations are presented in Section VI. Finally, Section VII concludes this paper.

II. Visible Light Indoor Positioning System

In this paper, we consider a VLP system with M $(M \geq 3)$ transmitters (LEDs) and one single receiver (PD). At the transmitter's side, the LEDs are uniformly distributed in the ceiling. For example, when considering the case of $M = 4$, the layout of LED distributions is displayed in Fig. 1(b). Besides, we assume that the different LEDs transmit signals at different time slots so that in each time slot the receiver can only detect the signal from one LED.

At the receiver's side, a receiver (PD) detects the optical signal and outputs the RSS of all LEDs (this can be done since the signals from different LEDs are transmitted at different time slots). Moreover, we assume no cross-talk between the signals from different LEDs, implying that the received signals and the output RSS for different LEDs are statistically independent. Besides, we also assume that the positions of LEDs are known to the receiver. The goal of the VLP system is to accurately estimate the position of the receiver based on the received signals and positions of all LEDs.

The system diagram is displayed in Fig. 1(a). We assume all LEDs are pointing downwards and the receiver plane is pointing upwards. For the i-th LED, we denote its horizontal location by $\{X_i = [x_i, y_i]^T\}$, and the unknown receiver location by $L = [x, y]^T$. Let h be the height of the room.

Moreover, following the convention [29], we assume that the LED follows the Lambertian radiation pattern. Then the channel gain from the ith LED to the PD, denoted by h_i, can be described

by (1),

$$h_i = \begin{cases} \frac{A_r(m+1)}{2\pi d_i^2}\cos^m(\phi_i)\cos(\psi_i)g(\psi_i), & 0 \le \psi_i \le \Psi, \\ 0, & \text{otherwise.} \end{cases} \tag{1}$$

where A_r is the area of PD; ψ_i is the angle of incidence of PD; ϕ_i is the irradiation angle; Φ is the field of view of PD and m is the mode of Lambertian emission related to the LED semi-angle at half-power $\Phi_{1/2}$, which takes the form

$$m = -\frac{\log 2}{\log\cos\Phi_{1/2}}. \tag{2}$$

Additionally, the function $g(\psi)$ denotes the optical gain of an ideal non-imaging concentrator with internal refractive index n [30],

$$g(\psi) = \begin{cases} \frac{n^2}{\sin^2\Psi_c}, & 0 \le \psi \le \Psi_c, \\ 0, & \text{otherwise,} \end{cases} \tag{3}$$

where $\Psi_c \le \frac{\pi}{2}$ is the field-of-view (FOV) [30].

Let $s_i(t)$ be the signal transmitted from the i-th LED at time t and $r(t)$ be the received signal at time t, we have

$$r(t) = \sum_{i=1}^{M} \gamma_i s_i(t) + n(t), \tag{4}$$

where $n(t)$ denotes the noise and γ_i is the channel gain of the transmission link from the i-th LED to the receiver, which can be described as follows,

$$\gamma_i = R_p \frac{A_r(m+1)}{2\pi d_i^2} g(\psi_i)\cos^m(\phi_i)\cos(\psi_i)G, \tag{5}$$

where d_i is the distance between the ith LED and the receiver. In our work, we only consider the synchronous system. R_p is the responsivity of PD. G is the optical amplifier gain. To simplify the expression, we denote γ_i as the attenuation of the ith link from ith LED to PD. Moreover, transmitted signals from different LEDs are orthogonal.

We further consider the case that in each time slot the receiver can only detect the signal from one LED. Therefore, we can divide the entire time period into M intervals, within which the received signal takes the form

$$r_i = \gamma_i s_i + n_i$$

where without loss of generality we use r_i to denote the received signal at the time slot that attributes to the i-th LED, and n_i denotes the noise at that time slot. Following existing works on the signal model in VLP or VLC system [12], we consider two types of noise: shot noise (which is signal dependent) and thermal noise (independent of the signal). Generally speaking, these two types of noise are typically assumed to be statistically independent, and thus we have

$$n_i = n_i^{\text{th}} + n_i^{\text{sh}}, \tag{6}$$

$$n_i^{\text{th}} \sim \mathcal{N}(0, \sigma^2), \tag{7}$$

$$n_i^{\text{sh}} \sim \mathcal{N}(0, \zeta^2\gamma_i s_i) \tag{8}$$

TABLE I
VALUES OF PARAMETERS USED IN THIS PAPER

Symbol	Quantity	Value	Unit
q	electron charge	1.6×10^{-19}	C
I_{DC}	dark current	5	pA
I_2	noise bandwidth factor	0.562	
I_3	noise bandwidth factor	0.0868	
Γ	channel noise factor	1.5	
R_p	detector responsivity	0.4	A/W
B	equivalent noise bandwidth	800	MHz
G_0	open-loop voltage gain	10	
K	Boltzmann's constant	1.38×10^{-23}	
T_e	absolute temperature	300	K
A_r	detector effective area	0.2	cm^2
g_m	transconductance	30	m/s
$\Delta\lambda$	bandwidth of the optical filter	400	nm
P_{BS}	background spectral irradiance	5.8×10^{-6}	$\text{W/cm}^2\cdot\text{nm}$
$\Phi_{1/2}$	LED semi-angle at half-power	70	degree ($^\circ$)
P	transmitted power	5	W
Ψ_c	FOV	60	degree ($^\circ$)
G	Amplification factor	100	

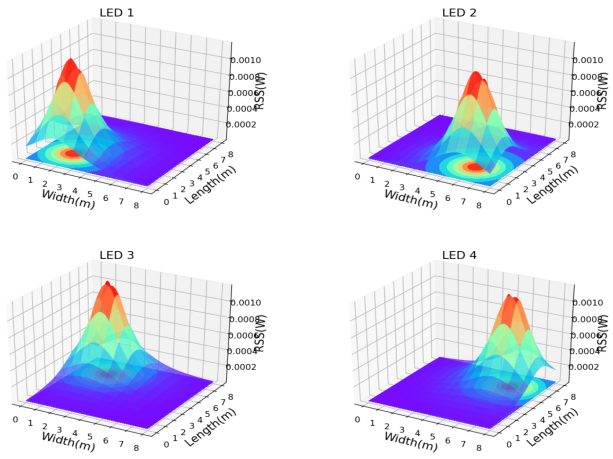

Fig. 2. RSS distribution of a VLP system with 4 LEDs.

where n_i, n_i^{th} and n_i^{sh} denote the total noise, thermal noise and shot noise at the time slot that attributes to the i-th LED, respectively. Moreover, following the convention, we assume that the thermal noise and shot noise satisfy Gaussian distributions. For the thermal and shot noises, we can calculate the quantities σ^2 and ζ^2 as follows [31], [32]

$$\sigma^2 = \frac{8\pi K T_e}{G_0}\eta A_r I_2 B^2 + \frac{16\pi^2 K T_e \Gamma}{g_m}\eta^2 A_r^2 I_3 B^3, \tag{9}$$

$$\zeta^2 = 2qR_p P_{rec} B. \tag{10}$$

where K, T_K is Boltzmann's constant; T_K is the absolute temperature; G_0, η, I_2, I_3, and P_{rec} are the device parameters of the PD. The exact definitions and values of these parameters are presented in Table I. We observe in (8) that the variance of the shot noise is proportional to the received signal strength. To better illustrate the signal model, we visualize the RSS distribution for a 4-LED VLP system in Fig. 2.

III. Problem Formulation and Gradient Descent Approach

In this section, we will formulate the positioning problem as an optimization problem and briefly explain the gradient descent approach, which has been widely implemented in practice, for solving this problem. We will also include the gradient method as a baseline algorithm that will be compared to the proposed algorithms in Section VI.

A. Problem Formulation

Let $L = [x, y]^T$ be the position of the receiver and $\{X_i = [x_i, y_i]^T\}$ be the position of the ith LED. Then let d_i be the distance between them, which satisfies

$$d_i^2 = (x_i - x)^2 + (y_i - y)^2 + h^2. \tag{11}$$

Recall that we assume that the receiver can detect the signals from all LEDs. Let $\boldsymbol{R} = (r_1, r_2, \ldots, r_M)$ be the collection of the received RSS of all LEDs,[1] then the posterior probability of L given $\boldsymbol{R}$ is defined as:

$$p(L|\boldsymbol{R}) = \frac{p(\boldsymbol{R}|L)p(L)}{p(\boldsymbol{R})}. \tag{12}$$

Further assume that L has a uniform prior (i.e., $p(L)$ is a constant) and $p(\boldsymbol{R})$ is invariant to all possible L. Hence, maximizing the posterior probability is equivalent to maximizing the likelihood $p(\boldsymbol{R}|L)$, i.e.,

$$\max p(L|\boldsymbol{R}) = \max p(\boldsymbol{R}|L). \tag{13}$$

Since in each time slot the receiver only detects the signal from one single LED, we have $r_1, \ldots, r_M$ are statistically independent. Therefore, it holds that

$$\begin{aligned} p(\boldsymbol{R}|L) &= p(r_1, r_2, \ldots, r_M|L) \\ &= \prod_{i=1}^{M} p(r_i|L). \end{aligned} \tag{14}$$

According to characteristics of channel gain (see (5)) and noises (see (9) and (8)), the PDF function $p(r_i|L)$ and the log-likelihood function $\Lambda(p(r_i|L))$ can be directly calculated, which we present in (15) and (16) respectively.

$$\begin{aligned} p(r_i|L) = &\frac{1}{\sqrt{2\pi(\sigma^2 + \zeta^2\gamma_i s_i)}} \exp\left\{-\frac{1}{2(\sigma^2 + \zeta^2\gamma_i s_i)}(r_i \right. \\ &\left. - \gamma_i s_i)^2\right\}, \end{aligned} \tag{15}$$

$$\begin{aligned} \Lambda(p(r_i|L) = &-\frac{(r_i - \gamma_i s_i)^2}{2(\sigma^2 + \zeta^2\gamma_i s_i)} - \frac{1}{2}\log(2\pi(\sigma^2 + \zeta^2\gamma_i s_i), \\ = &-\frac{\left(r_i - \frac{R_p A_R(m+1)h^{m+1}}{2\pi d_i^{m+3}} s_i\right)^2}{2\left(\sigma^2 + \zeta^2 \frac{R_p A_R(m+1)h^{m+1}}{2\pi d_i^{m+3}} s_i\right)} \\ &- \frac{1}{2}\log\left(2\pi\left(\sigma^2 + \zeta^2 \frac{R_p A_R(m+1)h^{m+1}}{2\pi d_i^{m+3}} s_i\right)\right). \end{aligned} \tag{16}$$

[1]In this paper we only consider using M RSS to estimate the receiver's position. In practice, we can utilize multiple rounds of RSS (i.e., the receiver collects kM signals if using k rounds) to further improve the positioning accuracy.

Then the goal is to find the optimal position parameter (x^*, y^*) to achieve maximum log-likelihood:

$$(x^*, y^*) = \arg\max_{x,y} \sum_{i=1}^{M} \Lambda(p(r_i|L)). \tag{17}$$

or,

$$(x^*, y^*) = \arg\min_{x,y} -\sum_{i=1}^{M} \Lambda(p(r_i|L)). \tag{18}$$

where M denotes the number of LEDs.

B. Gradient Descent Algorithm

Let $f(x, y)$ define the negative likelihood function

$$f(L) = -\sum_{i=1}^{M} \Lambda(p(r_i|L)), \tag{19}$$

where $L = [x, y]^\top$ is a collection of all location parameters. the next goal is to develop some efficient numerical algorithm to find the minimizer of $f(L)$. One standard and commonly used approach is gradient descent, which makes use of the gradient information to update the position parameter $L = [x, y]^\top$ in an iterative manner. In particular, we first write down the formula of the gradient as follows,

$$\nabla f(L) = \begin{bmatrix} \frac{\partial f}{\partial x} & \frac{\partial f}{\partial y} \end{bmatrix}. \tag{20}$$

and then the GD algorithm applies the following update rule,

$$L^{(t+1)} = L^{(t)} - \alpha \nabla f(L^{(t)}), \tag{21}$$

where α is the learning rate.

However, the major drawback of applying GD in the positioning system is that the negative log-likelihood function $f(L)$ is nonconvex with respect to the location parameter L (since the variance of shot noise also depends on L), which implies that GD could be easily trapped into some bad local minima or even saddle points, making the positioning results inaccurate. In order to alleviate this issue, we consider using the nearest neighbors (NN) strategy as initialization in [33], i.e., setting the initial location L as the position of the LED with the strongest received signal. Intuitively, NN can give a better positioning prediction (but the error is not tolerable), since that the NN initialization is closer to the optimum compared to the random guess. As a result, GD is more likely to converge to the global optimum since the loss function around the optimum is typically more convex. The numerical results will be reported in Section VI.

IV. Iterative Least Square Positioning

In this section, we propose a novel and more powerful approach for VLC positioning. We will show that the proposed approach is not only efficient but also can be effectively adapted to the GD algorithm to improve positioning accuracy further.

Recall that the received signal from the i-th LED takes the form

$$r_i = \gamma_i s_i + n_i. \tag{22}$$

where γ_i is the link gain, s_i is the transmitted signal, and n_i is a signal-dependent noise. Note that we have

$$\cos(\phi_i) = \cos(\psi_i) = \frac{h}{d_i}, \tag{23}$$

which implies that the link gain γ_i can be reformulated by

$$\gamma_i = \frac{R_p A_R (m+1)}{2\pi h^2} \cos^{m+3}(\phi_i). \tag{24}$$

Since the parameters R_p, A_R, m, and h are invariant to the positions of the receiver and LEDs, we further define $\Gamma = R_p A_R(m+1)/(2\pi h^2)$, and thus,

$$r_i = \Gamma \cos^{m+3}(\phi_i) s_i + n_i. \tag{25}$$

Assuming sufficiently high SNR, i.e., the variance of the noise n_i is significantly smaller than the magnitude of $\Gamma \cos^{m+3}(\phi_i) s_i$, applying first-order Taylor expansion we obtain

$$\left(\frac{r_i}{\Gamma s_i}\right)^{-\frac{2}{m+3}} = \frac{1}{\cos^2(\phi_i)} - \frac{2n_i}{\Gamma(m+3)\cos^{m+5}(\phi_i) s_i} + o\left(\frac{n_i}{\Gamma s_i}\right). \tag{26}$$

Note that the above equality holds for all $i \in [M]$, and our goal is to leverage those M qualities to solve for the position of the receiver (x, y). In order to achieve this, we will follow the similar idea in [34] by linearizing the target parameter (x, y). Specifically, note that the elevation angle ϕ_i satisfies

$$\cos^2(\phi_i) = \frac{h^2}{d_i^2} = \frac{h^2}{(x-x_i)^2 + (y-y_i)^2 + h^2} = \frac{h^2}{x^2 + y^2 - 2x_i x - 2y_i y + x_i^2 + y_i^2 + h^2}. \tag{27}$$

We define $\boldsymbol{\theta} = (x^2+y^2, x, y)^\top$ and $\mathbf{z}_i = (1, -2x_i, -2y_i)$. Then we have $\cos^2(\phi_i) = h^2/(\boldsymbol{\theta}^\top \mathbf{z}_i + x_i^2 + y_i^2 + h^2)$.

Therefore, the subsequent goal is to learn the vector $\boldsymbol{\theta}$ based on (26) for all $i \in [M]$. Note that n_i follows Gaussian distribution with zero mean and variance $\sigma^2 + \zeta^2 \gamma_i s_i$. Ignoring the high-order term $o\left(\frac{n_i}{\Gamma s_i}\right)$, given s_i and r_i, the likelihood function of $\boldsymbol{\theta}$ is given by (28),

$$p(\boldsymbol{\theta}|s_i, r_i) = \frac{1}{\sqrt{2\pi\hat{\sigma}_i^2}} \exp\left(-\frac{[\boldsymbol{\theta}^\top \mathbf{z}_i + x_i^2 + y_i^2 + h^2 - h^2 (r_i/\Gamma s_i)^{-2/(m+3)}]^2}{2\hat{\sigma}_i^2}\right), \tag{28}$$

where the variance $\hat{\sigma}_i^2$ is defined by

$$\hat{\sigma}_i^2 = \frac{4(\sigma^2 + \zeta^2 \gamma_i s_i)}{\Gamma^2 (m+3)^2 \cos^{2(m+5)}(\phi_i) s_i^2}. \tag{29}$$

Then the maximum likelihood solution $\boldsymbol{\theta}^*$ can be obtained by solving the following optimization problem

$$\boldsymbol{\theta}^* = \arg\max_{\boldsymbol{\theta}} \sum_{i=1}^{M} \log p(\boldsymbol{\theta}|s_i, r_i), \tag{30}$$

which is reformulated in detail in (31).

$$\boldsymbol{\theta}^* = \arg\max_{\boldsymbol{\theta}} \sum_{i=1}^{M} \left(\frac{\left[\boldsymbol{\theta}^\top \mathbf{z}_i + x_i^2 + y_i^2 + h^2 - h^2 (r_i/s_i)^{-2/(m+3)}\right]^2}{2\hat{\sigma}_i^2} + \log(\hat{\sigma}_i) \right). \tag{31}$$

Consider the case of high SNR, $\log(\hat{\sigma}_i)$ is typically much smaller than the first one, therefore we aim to solve the following approximate optimization problem

$$\boldsymbol{\theta}^* \approx \arg\max_{\boldsymbol{\theta}} \sum_{i=1}^{M} \frac{1}{2\hat{\sigma}_i^2} \cdot \left[\boldsymbol{\theta}^\top \mathbf{z}_i + x_i^2 + y_i^2 + h^2 - h^2 (r_i/s_i)^{-2/(m+3)}\right]^2 \tag{32}$$

However, the variance $\hat{\sigma}_i^2$ also depends on the target parameter $\boldsymbol{\theta}$ since ϕ_i is unknown and depends on (x, y), making the above optimization problem nonconvex and thus standard gradient descent may be intractable to find the optimal solution. In order to effectively solve the above problem, it requires an accurate estimation of $\hat{\sigma}_i^2$, or equivalently, a good estimation of (x, y).

A. The Least-Square Solver

In order to get a good estimation of $\hat{\sigma}_i^2$, we can first assume that $\hat{\sigma}_i$ is invariant for all LEDs, which translates (32) into a LS problem. In particular, we apply the method in [34] and aim to solve

$$\min_{\boldsymbol{\theta}} \|\mathbf{M}\boldsymbol{\theta} - \mathbf{b}\|_F^2,$$
$$\mathbf{M}_i = \mathbf{z}_i,$$
$$b_i = h^2 (r_i/s_i)^{-2/(m+3)} - (x_i^2 + y_i^2 + h^2).$$

The solution of this least square can be simply attained $\hat{\boldsymbol{\theta}} = (\mathbf{M}^\top \mathbf{M})^{-1} \mathbf{M}^\top \mathbf{b}$, which serves as a sub-optimal solution of (32).

B. Iterative LS Algorithm

Note that the LS solver ignores the difference between σ_i's for different i's, thus may not be able to provide sufficient accuracy. To tackle this problem, we can leverage the above LS solution $\hat{\boldsymbol{\theta}}$ to estimate the variance $\hat{\sigma}_i^2$. In the next step, we will further solve (32) with fixed $\hat{\sigma}_i^2$ in (29), which forms a new LS problem with updated $\mathbf{M}_i$'s and $\mathbf{b}_i$'s: $\mathbf{M}_i = \hat{\sigma}_i^{-2} \mathbf{z}_i$ and $b_i = \hat{\sigma}_i^{-2}[h^2 (r_i/s_i)^{-2/(m+3)} - (x_i^2 + y_i^2 + h^2)]$. Then the optimal solution obtained in the second step can be similarly solved using the closed-form solution $\hat{\boldsymbol{\theta}} = (\mathbf{M}^\top \mathbf{M})^{-1} \mathbf{M}^\top \mathbf{b}$.

Beyond the two-step solver, we can further extend this to multiple steps. In the initialization, we will set the same variance

Algorithm 1: Iterative LS Algorithm.

input: Received signals $\{r_i\}_{i=1,\dots,M}$, transmitted signals $\{s_i\}_{i=1,\dots,M}$, positions of LEDs $\{(x_i, y_i)\}_{i=1,\dots,M}$, height of the room h, number of iterations K.
initialization: Set $\hat{\sigma}_i = 1$ for all $i \in [M]$.
for $k = 0, 1, \dots, K$ **do**
Construct the matrix $\mathbf{M}$ and vector $\mathbf{b}$ such that
$\mathbf{M}_i = \hat{\sigma}_i^{-2}\mathbf{z}_i$ and
$b_i = \hat{\sigma}_i^{-2}[h^2(r_i/s_i)^{-2/(m+3)} - (x_i^2 + y_i^2 + h^2)]$
Compute the solution of the LS problem
$\boldsymbol{\theta}^{(k)} = (\mathbf{M}^\top\mathbf{M})^{-1}\mathbf{M}^\top\mathbf{b}$
Update the variances $\hat{\sigma}_i$ based on $\boldsymbol{\theta}^{(k)}$ and (29).
end for
output: $\boldsymbol{\theta}^{(K)}$

Algorithm 2: LS-GD Algorithm.

input: Received signals $\{r_i\}_{i=1,\dots,M}$, transmitted signals $\{s_i\}_{i=1,\dots,M}$, positions of LEDs $\{(x_i, y_i)\}_{i=1,\dots,M}$, height of the room h, learning rate α, stopping parameter ϵ.
LS Initialization: $\mathbf{z}_i = (1, -2x_i, -2y_i)$, $\mathbf{M}_i = \mathbf{z}_i$, $b_i = h^2(r_i/s_i)^{-2/(m+3)} - (x_i^2 + y_i^2 + h^2)$, then LS solution: $\hat{\boldsymbol{\theta}} = (\mathbf{M}^\top\mathbf{M})^{-1}\mathbf{M}^\top\mathbf{b}$ and $L^{(0)}$.
GD Process:
while $|f(L^{(t)}) - f(L^{(t-1)})| \le \epsilon$ **do**
$t = t + 1$
Update $L^{(t)}$ $L^{(t)} = L^{(t-1)} + \alpha\nabla f(L^{(t-1)})$.
end while
output: $\hat{L}$

parameter $\hat{\sigma}_i$ for all LEDs. In each iteration, we will first compute the variance parameter using the learned $\hat{\boldsymbol{\theta}}$ in the previous step, and then form the matrix $\mathbf{M}$ and vector $\mathbf{b}$ accordingly. Then using the closed-form solution of the LS problem to update $\hat{\boldsymbol{\theta}}$. We summarize the entire procedures in Algorithm 1. Then, we can update the $\hat{\sigma}_i^2$ with the updated $\hat{\boldsymbol{\theta}}$ and reformulate the problem iteratively until the solution converges.

C. LS-GD Algorithm

Recall that GD may be trapped by some bad local minima due to the non-convexity of the objective (32). Instead, one may need a quite good initial guess of the receiver's position to make it work effectively. Therefore, a natural idea is to combine the LS algorithm with the GD approach by using the solution found by the LS algorithm as the initialization of GD. This gives rise to the LS-GD algorithm, which is summarized in Algorithm 2.

V. Cramér-Rao Lower Bounds

Previous work [27] has studied the CRLB of distance estimation error, and theoretically revealed that shot noise affects positioning accuracy. In this section, we compute the CRLB of positioning error for VLP under thermal noise and shot noise. Thus, we can compare the positioning accuracy of the proposed algorithms with the theoretical lower bound.

Note that we aim to derive the CRLB of the position estimate $L = (\hat{x}, \hat{y})^\top$, by (16), the log-likelihood function of $L = (\hat{x}, \hat{y})$ is given by

$$\begin{aligned}\Lambda(L) &= -\sum_{i=1}^{M}\Lambda(p(r_i|L)) \\ &= -\sum_{i=0}^{M}\frac{(r_i - \gamma_i s_i)^2}{2(\sigma^2 + \zeta^2\gamma_i s_i)} - \frac{1}{2}\log(2\pi(\sigma^2 + \zeta^2\gamma_i s_i)\end{aligned} \tag{33}$$

where $\gamma_i = R_p A_R(m+1)/(2\pi h^2)\cos^{m+3}(\phi_i)$ and $\phi_i = \arccos(h/d_i)$ denotes the elevation angle of the path from the i-th LED to the receiver. The CRLB is based on the inverse of the Fisher Information Matrix (FIM) for $\hat{L}$, which states that the covariance of the predictions is lower bounded by the reciprocal of the Fisher information, i.e.,

$$\mathbb{E}\left[(\hat{L} - L)(\hat{L} - L)^\top\right] \succeq \mathbb{E}[(\nabla\Lambda(L))(\nabla\Lambda(L))^\top]^{-1}. \tag{34}$$

Let $\mathcal{J}(L)$ be the Fisher information and note that L is a 2-dimensional vector, thus it follows that

$$\mathcal{J}(L) = \begin{bmatrix}\mathbb{E}[(\nabla_x\Lambda(L))^2] & \mathbb{E}[(\nabla_x\Lambda(L))(\nabla_y\Lambda(L))] \\ \mathbb{E}[(\nabla_x\Lambda(L))(\nabla_y\Lambda(L))] & \mathbb{E}[(\nabla_y\Lambda(L))^2]\end{bmatrix} \tag{35}$$

Then using chain rule, let $v_i = \gamma_i s_i$ and $\Lambda_i = \Lambda(p(r_i|L))$, we have

$$\nabla_x\Lambda(L) = -\sum_{i=1}^{M}\frac{\partial\Lambda_i}{\partial v_i}\frac{\partial v_i}{\partial x}. \tag{36}$$

Note that given ∂v_i does not rely on the random observation r_i, thus when calculating the fisher information we only need to take expectation over the randomness in $\partial\Lambda_i/\partial v_i$. Moreover, since r_i and $r_{i'}$ are independent if $i \neq i'$, it is easy to verify that $\mathbb{E}[(\partial\Lambda_i/\partial v_i)(\partial\Lambda_{i'}/\partial v_{i'})] = 0$. Then we have (37).

$$\begin{aligned}\mathbb{E}\left[(\nabla_x\Lambda(L))^2\right] &= \mathbb{E}\left[\left(\sum_{i=1}^{M}\frac{\partial\Lambda_i}{\partial v_i}\frac{\partial v_i}{\partial x}\right)^2\right] \\ &= \sum_{i=1}^{M}\mathbb{E}\left[\left(\frac{\partial\Lambda_i}{\partial v_i}\right)^2\right]\left(\frac{\partial v_i}{\partial x}\right)^2.\end{aligned} \tag{37}$$

Note that r_i follows Gaussian distribution with mean $\gamma_i s_i$ and variance $\sigma^2 + \zeta^2\gamma_i s_i$, it can be derived that

$$\mathbb{E}\left[\left(\frac{\partial\Lambda_i}{\partial v_i}\right)^2\right] = \frac{\zeta^4 + 2(\sigma^2 + \zeta^2\gamma_i s_i)}{2(\sigma^2 + \zeta^2\gamma_i s_i)^2}. \tag{38}$$

Moreover, recall that $d_i = \sqrt{(x - x_i)^2 + (y - y_i)^2 + h^2}$, we further calculate (39).

$$\begin{aligned}\frac{\partial v_i}{\partial x} &= -\frac{R_p A_R(m+1)(m+3)\cos^{m+3}(\phi_i)(x - x_i)}{2\pi h^2 d_i^2}s_i \\ &= \frac{(m+3)\gamma_i s_i(x - x_i)}{d_i^2}.\end{aligned} \tag{39}$$

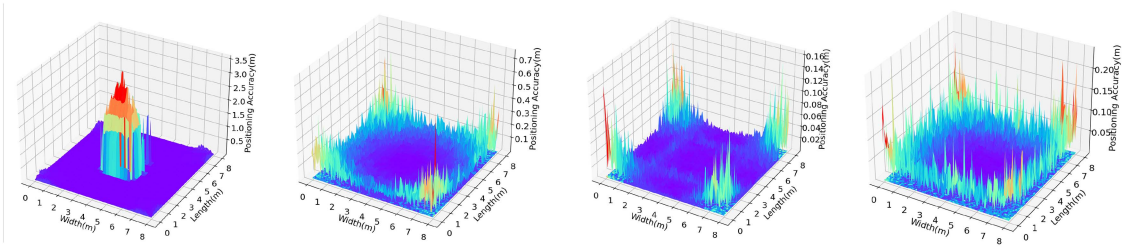

(a) SGDM (b) LS (c) LS-GD (d) Iterative LS

Fig. 3. Visualization of the positioning accuracy of different positioning algorithms, including GD, LS, LS-GD, iterative GD, in 8 m $\times$ 8 m room.

Therefore, combining the above results we can obtain (40), (41), and (42).

$$\mathbb{E}\left[(\nabla_x \Lambda(L))^2\right] = \sum_{i=1}^{M} \frac{\zeta^4 + 2(\sigma^2 + \zeta^2\gamma_i s_i)}{2(\sigma^2 + \zeta^2\gamma_i s_i)^2} \left(\frac{(m+3)\gamma_i s_i}{d_i^2}\right)^2 (x - x_i)^2, \tag{40}$$

$$\mathbb{E}\left[(\nabla_y \Lambda(L))^2\right] = \sum_{i=1}^{M} \frac{\zeta^4 + 2(\sigma^2 + \zeta^2\gamma_i s_i)}{2(\sigma^2 + \zeta^2\gamma_i s_i)^2} \left(\frac{(m+3)\gamma_i s_i}{d_i^2}\right)^2 (y - y_i)^2, \tag{41}$$

$$\mathbb{E}\left[(\nabla_x \Lambda(L))(\nabla_y \Lambda(L))\right] = \sum_{i=1}^{M} \frac{\zeta^4 + 2(\sigma^2 + \zeta^2\gamma_i s_i)}{2(\sigma^2 + \zeta^2\gamma_i s_i)^2} \left(\frac{(m+3)\gamma_i s_i}{d_i^2}\right)^2 (x - x_i)(y - y_i). \tag{42}$$

At last, from FIM in (35), we can derive the lower bound of the expected estimation error $\mathbb{E}[(\hat{x} - x)^2 + (\hat{y} - y)^2]$ as following,

$$\mathbb{E}\left[(\hat{x} - x)^2 + (\hat{y} - y)^2\right] = \mathrm{Tr}\left(\mathbb{E}\left[(\hat{L} - L)(\hat{L} - L)^\top\right]\right) \geq \mathrm{Tr}\left(\mathcal{J}(L)^{-1}\right). \tag{43}$$

Accordingly, we can derive a close-form lower bound on the estimation error using (40), (41), (42) and (35).

VI. Numerical Results

In this section, we simulate GD, LS, LS-GD, and iterative LS positioning. Based on the derivation of CRLB in Section V, we also show the CRLB of VLP under thermal and shot noise. In our simulation, we assume an indoor place of 8 m $\times$ 8 m with LEDs uniformly distributed in the ceiling. The vertical distance between the ceiling and receiver is 2 m. The LED semi-angle at half-power is $\Phi_{1/2} = 70^\circ$ [30] and the transmitted power is 5 W. The amplification factor on the receiver side is 100. Other relevant parameters are given in the following table. We divide the room into 100×100 grids and calculate the positioning accuracy of each node of the room.

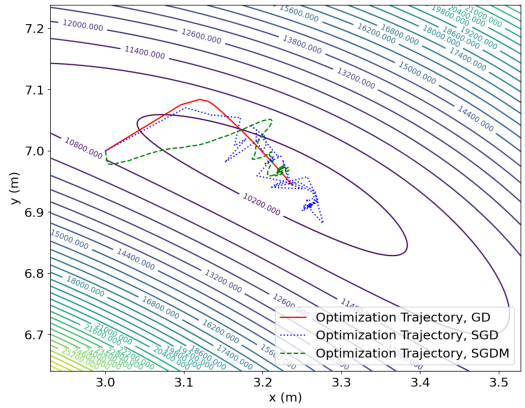

Fig. 4. Optimization trajectory of GD, SGD, and SGDM, suggesting that these three algorithms can be stuck at some spurious local minima.

A. Positioning Accuracy of Each Algorithm

In Fig. 3, we present the performance of four positioning algorithms, respectively. In Fig. 3(a), we simulate the positioning accuracy by the GD algorithm. The learning rate of the GD algorithm is set to 10^{-4} to guarantee stable convergence. The average positioning accuracy of the room and its variance are 0.131 m and 0.180 m ^{2} respectively. The average time cost is 0.157 s for each node. In the center of the room, it is the most overlapped area by four LEDs coverage. Thus the positioning performance is worst in the center due to the local minima issue of the GD algorithm. In Fig. 3(b), the positioning performance of the LS algorithm in the room is presented. The average positioning accuracy and variance are 0.046 m and 0.003 m^2 in the room and the computation time of each node is 2.98×10^{-5} s. The time cost is dramatically improved. But in four corners of the room, the positioning accuracy is the worst, because we ignore the high-order term which is more dominant in the corners. Furthermore, we simulate the LS-GD algorithm for positioning in Fig. 3(c). The average positioning accuracy is improved by 0.009 m, the variance is also improved to 1.86×10^{-5}m ^{2}, and it costs 0.046 s to locate each node. By implementing LS to initialize the GD algorithm, the time cost is improved and the average positioning accuracy is dramatically meliorated.

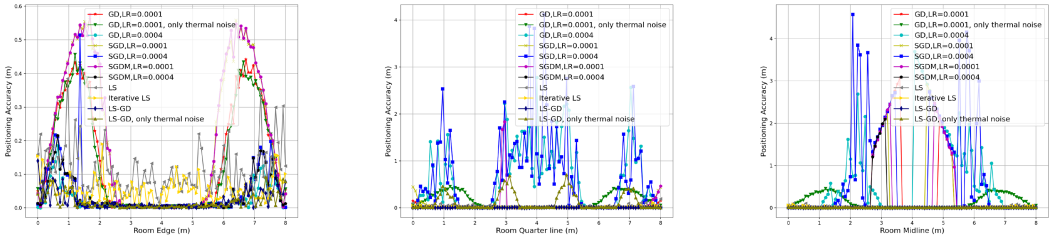

(a) The positioning accuracy of room edge of each algorithm (y-axis= 0m).

(b) The positioning accuracy of room quarter line of each algorithm (y-axis= 2m).

(c) The positioning accuracy of room midline of each algorithm (y-axis= 4m).

Fig. 5. Different positioning accuracy from different dimensions of the room.

TABLE II
COMPUTATION TIME AND AVERAGE POSITIONING ACCURACY OF DIFFERENT POSITIONING ALGORITHMS

Algorithm	GD (LR=0.0001)	GD (LR=0.0004)	SGD (LR=0.0001)	SGD (LR=0.0004)	SGDM (LR=0.0001)	SGDM (LR=0.0004)	GD (LR=0.0001, Only thermal noise)	LS	LS-GD (LR=0.0001)	LS-GD (LR=0.0001, Only thermal noise)	Iterative LS
Computation Time (s)	0.157	0.260	0.260	0.252	0.253	0.254	0.192	2.98×10^{-5}	0.046	0.896	1.94×10^{-4}
Average Positioning Accuracy (m)	0.131	0.718	0.161	0.706	0.214	0.113	0.257	0.046	0.009	0.092	0.023
Variance(m^2)	0.180	0.622	0.213	0.675	0.328	0.213	0.223	0.003	1.86×10^{-6}	0.024	6.05×10^{-4}

In Fig. 3(d), we show the simulation result of iterative LS positioning. The average positioning accuracy is 0.023 m, the variance is 6.05×10^{-4} m^2, and the time cost is 1.94×10^{-4}s. It can be seen that the iterative LS achieves the top-2 performance in terms of both time cost and positioning accuracy.

In addition to GD, we further consider its stochastic version, i.e. SGD as the baseline algorithm, which has been widely applied in many machine learning and optimization applications to achieve better performance. In particular, we consider two variants of the SGD algorithms: (1) SGD, which adds noise to the exact gradient and makes updates, and (2) SGD with momentum (SGDM), which incorporates the historical stochastic gradients into the calculation of current updates. Besides, we consider multiple choices of the learning rate (LR $\in \{0.0001, 0.0004\}$) for all gradient based optimization algorithms (i.e., GD, SGD, SGDM).

The detailed time costs and positioning accuracy of all algorithms are summarized in Table II. To sum up, the sub-optimal solution found by LS algorithm achieves the smallest time cost as it is only operated in one single step, but at the price of a relatively large positioning error. The GD algorithm has much worse positioning accuracy and computation time due to its slow convergence and inability to find the global optimum. Besides, using stochastic gradient, including SGD and SGM, and tuning learning rate cannot significantly improve the positioning accuracy achieved by GD, the best result among these stochastic gradient based algorithms (SGM with LR $= 0.0004$) can only achieve 0.113 m accuracy, which is still far from the positioning accuracy achieved by LS based algorithms. In fact, the reason of the worse positioning performance of GD, SGD, and SGDM lies in the fact that they are stuck at the spurious local minima of the training objective function. To show this, we pick a receiver position $(3.12, 4.88)$ (which is close to the middle of the room) that both GD, SGD, and SGDM fail to find the global minimum and lead to large positioning errors (while the LS based algorithms perform quite well, see Fig. 3(b)–(d)), and visualize the optimization trajectories of these three algorithms. The results are reported in Fig. 4. In particular, these three algorithms will converge to the point with training loss (i.e., negative log-likelihood) around 10^4. However, the optimal training loss, achieved around the true position $(3.12, 4.88)$, is -13.7, which is far smaller. This demonstrates that the point found by GD, SGD, and SGDM is indeed a spurious local minimum, which backups our previous reasoning.

Then remarkably, the GD algorithm can be dramatically improved in terms of both convergence and the optimality of the found solution by leveraging the LS solution as the initialization: the LS-GD method gives the best positioning error with much smaller running time. Moreover, the iterative LS algorithm makes a trade-off between time cost and positioning accuracy and gives the top-2 results in terms of both of these two criteria. Lastly, we also performed the positioning algorithms when ignoring the shot noise. It can be seen that the performance has been significantly downgraded. This demonstrates the importance and necessary of considering the shot noise in the VLP system.

B. *Impact of Shot Noise*

In this section, we also compared the simulation results of GD and LS-GD under only thermal noise, in which the impact of shot noise can be indicated. In Fig. 5(a), (b), and (c), the positioning accuracy of each algorithm in the columns of y-axis = 0 m, y-axis = 2 m, and y-axis = 4 m are presented, respectively. In Fig. 5(a), the positioning accuracy in the room edge (y-axis = 0 m) is shown. It can be seen the LS algorithm and LS-GD algorithm are worse than other algorithms, due to the signals being weaker in the room edge and some opponents being approximated and abandoned in LS and LS-GD algorithms. Fig. 5(b) presents the positioning accuracy of y-axis = 2 m. Recall that the room size is 8 m $\times$ 8 m and the 2D-coordinates of four LEDs are $(2, 2)$, $(2, 6)$, $(6, 6)$, and $(6, 2)$. It is noted that there are four

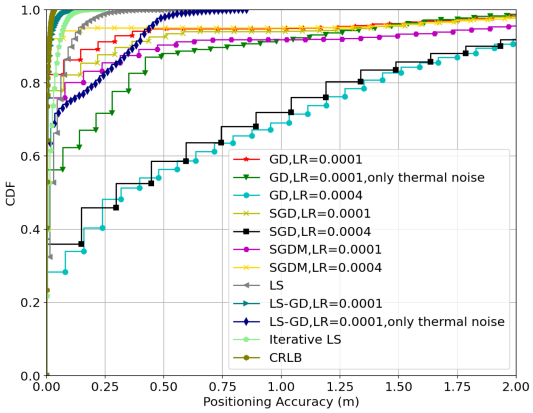

Fig. 6. Positioning accuracy comparison between different algorithms. Here we display the CDF of the positioning accuracy collected at the 100×100 grids.

peaks of GD and LS-GD algorithms under only thermal noise where it shows worse positioning accuracy of GD under only thermal noise and LS-GD under only thermal noise. The four peaks represent the areas where shot noise can affect positioning accuracy dramatically. The positioning accuracy of y-axis $= 4$ m in Fig. 5(c) is presented. It can be observed that in the center of the room the positioning performance of the GD algorithm and GD under only thermal noise is particularly inaccurate. It is because the RSS from each LED is comparatively close which can easily drag the GD algorithm into the local minima problem.

In Fig. 6, we show the cumulative distribution function (CDF) of the four algorithms above. From the perspective of positioning accuracy, the LS-GD algorithm outperforms other algorithms. Considering the trade-off between positioning accuracy and computation time, the iterative-LS algorithm is recommended for considerable average positioning accuracy and computation time.

VII. Conclusion

In this paper, we analyze the VLP system under shot noise and thermal noise. The simulation result reveals the conventional GD algorithm is expensive-time-cost and inaccurate. By tuning parameters like the learning rate, the performance is improved to a limited level by GD, SGD, and SGDM. To improve positioning performance, we propose the LS-GD algorithm. The first step is to utilize the LS algorithm to locate the initial position and then the GD algorithm proceeds. Thus by LS initializing, the GD process can shrink dramatically which saves positioning time to a large extent. By simulation, the average positioning accuracy of the LS-GD algorithm can achieve 0.009 m with a computation time of 0.046 s. In addition, based on the LS algorithm, we introduce an iterative LS algorithm that is both accurate and time-saving. The simulation results indicate that the iterative LS algorithm can achieve an average positioning accuracy of 0.023 m with 1.94×10^{-4}s computation time. Among the algorithms above, the local minimum can take place and result in poor positioning by the GD algorithm. According to the assumed VLP settings, we calculate the CRLB under the thermal and signal-dependent shot noise. The numerical results are provided to validate our proposed algorithms.

Appendix
Proof of the Learning Step

By chain rule, the derivation of $\frac{\partial \Lambda(p(r_i|L))}{\partial x}$ can be divided into three opponents as follows,

$$\frac{\partial \Lambda(p(r_i|L))}{\partial x} = \frac{\partial \Lambda(p(r_i|L))}{\partial \upsilon_i}\frac{\partial \upsilon_i}{\partial d_i}\frac{\partial d_i}{\partial x}. \tag{44}$$

$$\frac{\partial \Lambda(p(r_i|L))}{\partial \upsilon_i} = \frac{\zeta^2 s_i (r_i - \gamma_i s_i)^2}{2(\sigma^2 + \zeta^2 \gamma_i s_i)^2} + \frac{s_i (r_i - \gamma_i s_i)}{\sigma^2 + \zeta^2 \gamma_i s_i} - \frac{\zeta^2 s_i}{2(\sigma^2 + \zeta^2 \gamma_i s_i)}, \tag{45}$$

$$\frac{\partial \upsilon_i}{\partial d_i} = -\frac{(m+3)(m+1) R_p A_R h^{m+1}}{2\pi d_i^{(m+4)}}, \tag{46}$$

$$\frac{\partial d_i}{\partial x} = \frac{x - x_i}{\sqrt{(x_i - x)^2 + (y_i - y)^2 + h^2}} \tag{47}$$

$$\frac{\partial d_i}{\partial y} = \frac{y - y_i}{\sqrt{(x_i - x)^2 + (y_i - y)^2 + h^2}}. \tag{48}$$

References

[1] E. Kaplan and C. Hegarty, *Understanding GPS: Principles and Applications*. Norwood, MA, USA: Artech House, 2005.

[2] S. Cincotta, C. He, A. Neild, and J. Armstrong, "Indoor visible light positioning: Overcoming the practical limitations of the quadrant angular diversity aperture receiver (QADA) by using the two-stage QADA-plus receiver," *Sensors*, vol. 19, no. 4, 2019, Art. no. 956.

[3] Y. Zhuang, Z. Syed, Y. Li, and N. El-Sheimy, "Evaluation of two WiFi positioning systems based on autonomous crowdsourcing of handheld devices for indoor navigation," *IEEE Trans. Mobile Comput.*, vol. 15, no. 8, pp. 1982–1995, Aug. 2016.

[4] P. Bahl and V. N. Padmanabhan, "Radar: An in-building RF-based user location and tracking system," in *Proc. IEEE Conf. Comput. Commun. 19th Annu. Joint Conf. IEEE Comput. Commun. Soc.*, vol. 2, 2000, pp. 775–784.

[5] A. M. Hossain and W.-S. Soh, "A comprehensive study of bluetooth signal parameters for localization," in *Proc. IEEE 18th Int. Symp. Pers., Indoor Mobile Radio Commun.*, 2007, pp. 1–5.

[6] Y. Zhuang, J. Yang, Y. Li, L. Qi, and N. El-Sheimy, "Smartphone-based indoor localization with bluetooth low energy beacons," *Sensors*, vol. 16, no. 5, 2016, Art. no. 596.

[7] A. R. J. Ruiz, F. S. Granja, J. C. P. Honorato, and J. I. G. Rosas, "Accurate pedestrian indoor navigation by tightly coupling foot-mounted IMU and RFID measurements," *IEEE Trans. Instrum. Meas.*, vol. 61, no. 1, pp. 178–189, Jan. 2012.

[8] P. Yang and W. Wu, "Efficient particle filter localization algorithm in dense passive RFID tag environment," *IEEE Trans. Ind. Electron.*, vol. 61, no. 10, pp. 5641–5651, Oct. 2014.

[9] S.-H. Fang, C.-H. Wang, T.-Y. Huang, C.-H. Yang, and Y.-S. Chen, "An enhanced ZigBee indoor positioning system with an ensemble approach," *IEEE Commun. Lett.*, vol. 16, no. 4, pp. 564–567, Apr. 2012.

[10] H. Haas et al., "Wireless data from every light bulb," TED, 2011. [Online]. Available: https://www.ted.com/search?q=wireless+data+from+every+light+bulb

[11] *IEEE Standard for Local and Metropolitan Area Networks–Part 15.7: Short-Range Wireless Optical Communication Using Visible Light*, IEEE Standard 802.15.7-2011, 2011.

[12] Y. Zhuang et al., "A survey of positioning systems using visible led lights," *IEEE Commun. Surveys Tuts.*, vol. 20, no. 3, pp. 1963–1988, Jul.–Sep. 2018.

[13] N. U. Hassan, A. Naeem, M. A. Pasha, T. Jadoon, and C. Yuen, "Indoor positioning using visible led lights: A survey," *ACM Comput. Surv.*, vol. 48, no. 2, pp. 1–32, 2015.

[14] J. Luo, L. Fan, and H. Li, "Indoor positioning systems based on visible light communication: State of the art," *IEEE Commun. Surveys Tut.*, vol. 19, no. 4, pp. 2871–2893, Oct.–Dec. 2017.

[15] B. Zhu, J. Cheng, Y. Wang, J. Yan, and J. Wang, "Three-dimensional VLC positioning based on angle difference of arrival with arbitrary tilting angle of receiver," *IEEE J. Sel. Areas Commun.*, vol. 36, no. 1, pp. 8–22, Jan. 2018.

[16] P. Du et al., "Experimental demonstration of 3-D visible light positioning using received signal strength with low-complexity trilateration assisted by deep learning technique," *IEEE Access*, vol. 7, pp. 93986–93997, 2019.

[17] S. Zhang, P. Du, C. Chen, and W.-D. Zhong, "3-D indoor visible light positioning system using RSS ratio with neural network," in *Proc. IEEE 23rd Opto-Electron. Commun. Conf.*, 2018, pp. 1–2.

[18] K. Majeed and S. Hranilovic, "Passive indoor visible light positioning system using deep learning," *IEEE Internet Things J.*, vol. 8, no. 19, pp. 14810–14821, Oct. 2021.

[19] N. Knudde, W. Raes, J. De Bruycker, T. Dhaene, and N. Stevens, "Data-efficient Gaussian process regression for accurate visible light positioning," *IEEE Commun. Lett.*, vol. 24, no. 8, pp. 1705–1709, Aug. 2020.

[20] M. F. Keskin, E. Gonendik, and S. Gezici, "Improved lower bounds for ranging in synchronous visible light positioning systems," *J. Lightw. Technol.*, vol. 34, no. 23, pp. 5496–5504, Dec. 2016.

[21] M. F. Keskin and S. Gezici, "Comparative theoretical analysis of distance estimation in visible light positioning systems," *J. Lightw. Technol.*, vol. 34, no. 3, pp. 854–865, Feb. 2016.

[22] Y. Qi and H. Kobayashi, "Cramer-rao lower bound for geolocation in non-line-of-sight environment," in *Proc. IEEE Int. Conf. Acoust., Speech, Signal Process.*, 2002, vol. 3, pp. III–2473.

[23] X. Zhang, J. Duan, Y. Fu, and A. Shi, "Theoretical accuracy analysis of indoor visible light communication positioning system based on received signal strength indicator," *J. Lightw. Technol.*, vol. 32, no. 21, pp. 3578–3584, Nov. 2014.

[24] X. Sun, J. Duan, Y. Zou, and A. Shi, "Impact of multipath effects on theoretical accuracy of TOA-based indoor VLC positioning system," *Photon. Res.*, vol. 3, no. 6, pp. 296–299, 2015.

[25] M. F. Keskin, S. Gezici, and O. Arikan, "Direct and two-step positioning in visible light systems," *IEEE Trans. Commun.*, vol. 66, no. 1, pp. 239–254, Jan. 2018.

[26] T. Borogovac, M. B. Rahaim, M. Tuganbayeva, and T. D. Little, "'Lights off' visible light communications," in *Proc. IEEE GLOBECOM Workshops*, 2011, pp. 797–801.

[27] X. Liu, D. Zou, N. Huang, and S. Zhang, "A comprehensive accuracy analysis of visible light positioning under shot noise," in *Proc. IEEE/CIC Int. Conf. Commun. China*, 2020, pp. 167–172.

[28] V. Varshney, R. K. Goel, and M. A. Qadeer, "Indoor positioning system using Wi-Fi bluetooth low energy technology," in *Proc. IEEE 13th Int. Conf. Wireless Opt. Commun. Netw.*, 2016, pp. 1–6.

[29] I. Moreno and C.-C. Sun, "Modeling the radiation pattern of LEDs," *Opt. Exp.*, vol. 16, no. 3, pp. 1808–1819, 2008.

[30] Z. Ghassemlooy, W. Popoola, and S. Rajbhandari, *Optical Wireless Communications: System and Channel Modelling With Matlab*. Boca Raton, FL, USA: CRC press, 2019.

[31] T. Komine and M. Nakagawa, "Fundamental analysis for visible-light communication system using LED lights," *IEEE Trans. Consum. Electron.*, vol. 50, no. 1, pp. 100–107, Feb. 2004.

[32] H. Manor and S. Arnon, "Performance of an optical wireless communication system as a function of wavelength," *Appl. Opt.*, vol. 42, no. 21, pp. 4285–4294, 2003.

[33] L. Yunxiao and Q. Sujuan, "An improved indoor positioning method based on received signal strengths," in *Proc. Int. Conf. Intell. Transp., Big Data Smart City*, 2015, pp. 90–93.

[34] D. Li, C. Gong, and Z. Xu, "A rssi-based indoor visible light positioning approach," in *Proc. IEEE 10th Int. Symp. Commun. Syst., Netw. Digit. Signal Process.*, 2016, pp. 1–6.